ACS OMEGA

Open Access



http://pubs.acs.org/journal/acsodf

Article

# Dual Stimuli-Responsive Nanoprecursor of Ascorbic Acid and Quinone Methide Disrupting Redox Homeostasis for Cancer Treatment

Anup Dey, Pramod Kumar E. K., Chan Ho Kim, Yuce Li,* and Jae Hyung Park*

Cite This: *ACS Omega* 2024, 9, 32124−32132

Read Online

ACCESS | Metrics & More | Article Recommendations | Supporting Information

**ABSTRACT:** Disrupting the redox balance through reactive oxygen species (ROS) generation and intracellular glutathione (GSH) depletion presents a promising strategy for cancer therapy. Megadoses of ascorbic acid (AA) can induce oxidative stress in cancer cells, leading to cell death. However, achieving enhanced oxidative stress using ultrahigh doses of AA is challenging because of the intricate delivery of high-concentration AA to the targeted sites while the cancer cells could also re-establish more robust redox homeostasis by upregulating antioxidants such as GSH. Recently, quinone methide and its analogues (QMs) have been recognized as effective GSH scavengers, offering a new dimension to accelerate oxidative stress. In this study, we formulated a dual stimuli-responsive nanoprecursor of AA and QM using gold nanoparticles. The nanoprecursor can release AA in response to the intracellular acidic pH in tumor cells, elevating the intracellular ROS levels and triggering the production of ample QMs to quench excessive GSH. This positive feedback mechanism significantly amplifies oxidative stress and disrupts redox homeostasis in cancer cells at a relatively low concentration of AA, leading to selective apoptosis without affecting normal cells. These results highlight the potential of the nanoprecursor as an effective anticancer therapeutic.

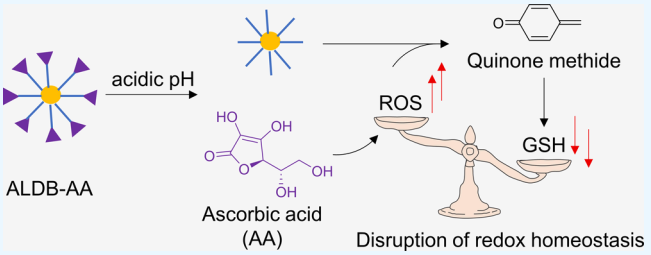


## INTRODUCTION

Cellular redox homeostasis—a vital and dynamic state that maintains the equilibrium between reduction and oxidation reactions within cells—governs several biological reactions and cellular processes, such as energy production, cell signaling, and survival.[1−4] Oxidative stress is an intricate state in which redox homeostasis is disrupted, characterized by an imbalance between the increased reactive oxygen species (ROS) generation and efficiency of the antioxidant defense system.[5,6] Oxidative stress can damage cellular components such as DNA and proteins, thus presenting an intriguing avenue for potential cancer therapy.[7,8]

Ascorbic acid (AA), also known as vitamin C, is a cost-effective but indispensable water-soluble vitamin.[9] Recent studies suggest that an ultrahigh pharmacological dose (800−1000 times the daily recommended intake) of AA can be a potential cancer therapeutic because it prompts cancer cells to generate ROS.[10,11] While the precise mechanism remains under investigation, hints allude to its potential role in modulating intracellular iron metabolism, subsequently contributing to the formation of hydroxyl radicals through the Fenton reaction.[12] Despite evidence supporting the safety of high-dose vitamin C administration, endogenous regulatory mechanisms inherently maintain it within physiologically optimal bounds, rendering this approach for cancer treatment impractical. Additionally, at diminished concentrations, AA predominantly acts as an antioxidant. For example, at serum concentrations of 40−80 $\mu$M, it exhibits notable efficacy in diminishing low-density lipoprotein oxidation associated with atherosclerosis and cell membrane lipid oxidation.[13,14] This dichotomous behavior highlights the need for targeted delivery of high-dose AA to tumor cells to harness its ROS-inducing capability for instigating cancer cell death. Nanoparticle-based drug delivery systems have displayed the ability to target high concentrations of cargos to cancer cells and accelerate the uptake of small molecules. In particular, gold nanoparticles stand out because they offer uniform size distribution and tunable surface properties. Chakraborty and Jana.[15] developed two ascorbic acid-conjugated nanoparticles and discovered that the delivery of ascorbic acid via these nanoparticles could induce cell death at millimolar concentrations (2−10 mM) by inducing oxidative stress.

Cells are equipped with a robust defense mechanism to maintain a physiologically balanced level of ROS.[16,17] When confronted with elevated intracellular ROS levels, they could

Received: May 4, 2024
Revised: June 14, 2024
Accepted: June 20, 2024
Published: July 15, 2024

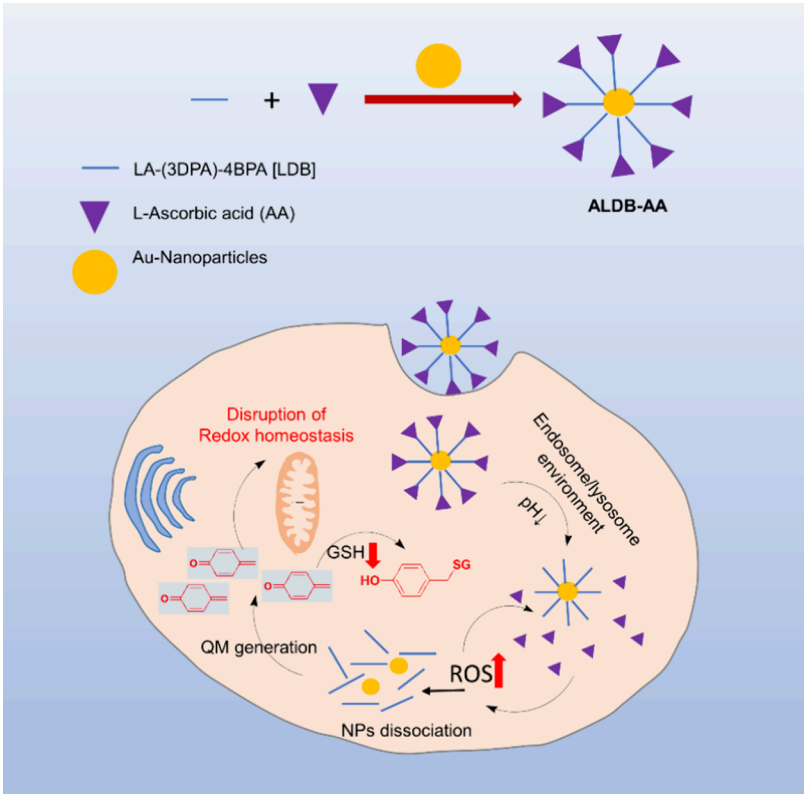


**Figure 1.** Schematic illustration of a dual-stimuli-responsive nanoprecursor (ALDB-AA) formulation and disruption of redox homeostasis for cancer treatment. NPs, nanoparticles; QM, quinone methide; ROS, reactive oxygen species; GSH, glutathione.

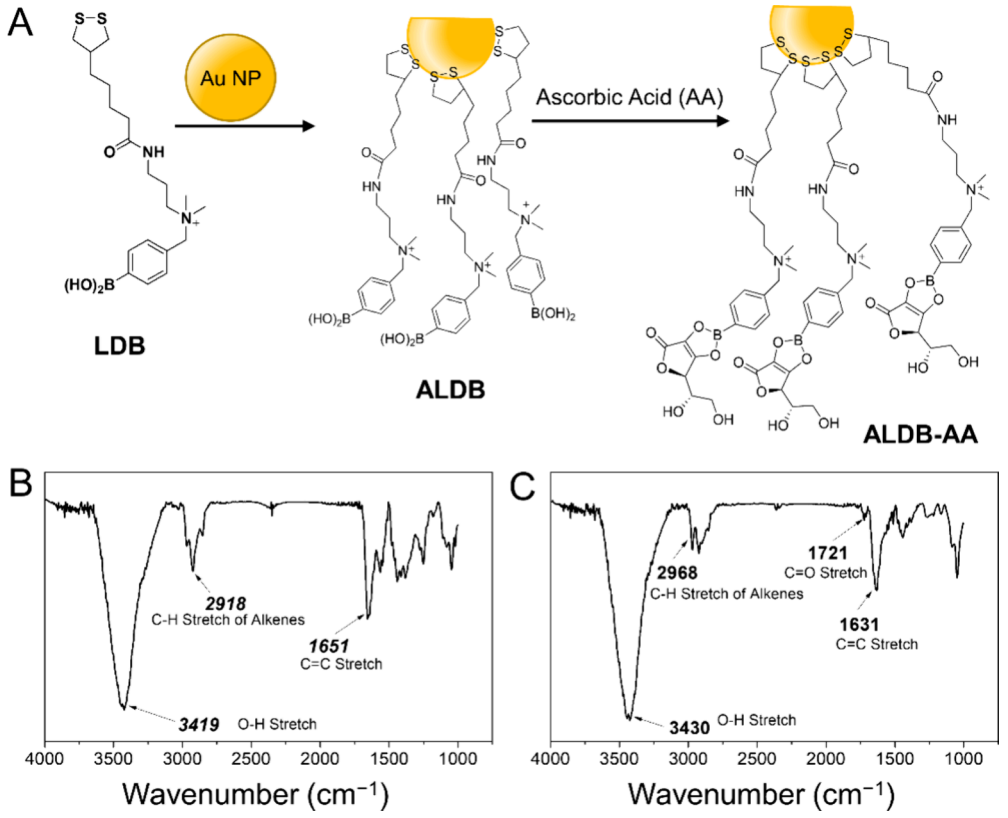


**Figure 2.** (A) Synthesis of ALDB-AA. (B, C) FT-IR spectroscopy of ALDB (B) and ALDB-AA (C).

re-establish more robust redox homeostasis using various signal pathways that convert highly reactive free radicals into less harmful molecules and elevate their ROS tolerance threshold.[18] This process involves the upregulation of antioxidants



https://doi.org/10.1021/acsomega.4c04260
ACS Omega 2024, 9, 32124−32132

such as glutathione (GSH) and augmented production of enzymes such as superoxide dismutase, instrumental in ROS decomposition.[19,20] These protective strategies enable tumor cells to survive, even though they often exhibit higher ROS levels compared to normal cells owing to their rapid metabolism.[21,22] Diminishing antioxidant levels, such as GSH, would revoke such protection mechanisms and has shown an association with cancer cell death.[23,24] Quinone methide (QM) and its derivatives possess the ability to alkylate intracellular thiol-bearing reductive molecules, including GSH, considered as promising therapeutics for disrupting redox homeostasis in cancer cells.[25,26] However, owing to their high reactivity, direct applications of QM remain challenging. As a result, stimuli-responsive precursors generating *in situ* QM are highly desired.[27,28]

In this study, we developed a dual-stimuli-responsive nanoprecursor of AA and QM using gold nanoparticles, termed ALDB-AA (Figure 1). This nanoprecursor is designed to release AA in response to the acidic intracellular pH of tumor cells and produce abundant QMs at the ROS level-elevated tumor cell microenvironment. Consequently, the released AA increases the ROS level in cancer cells, thereby enhancing QM generation to quench excessive GSH in the cancer cells. This positive feedback mechanism significantly amplifies oxidative stress and disrupts the redox homeostasis in cancer cells, causing selective apoptosis while sparing normal cells. Importantly, these effects were achieved at a relative low concentration (200−400 $\mu$M), which will make the anticancer application of ascorbic acid more practical.

## RESULTS AND DISCUSSION

**Preparation and Characterization of ALDB-AA.** To fabricate the nanoprecursor (ALDB-AA), the LDB was first anchored onto the gold nanoparticle surface by the inherent affinity between sulfur and gold. The successful synthesis of intermediates and the Au−S conjugation in ALDB were confirmed by $^1$H NMR and energy-dispersive spectrometry (EDS) mapping (Figures S1−S4). Subsequently, AA was tethered to the resultant nanoparticles using an esterification reaction between the boronic acid group and enediol groups of AA (Figure 2A).[29] The structure of ALDB and ALDB-AA was confirmed by FT-IR (Figure 2B,C). The appearance of the carbonyl stretching frequency of AA at 1721 cm$^{-1}$ indicated its successful conjugation. The content of AA was quantified to be 3.5% ($w/w$) through UV−vis spectroscopy and confirmed by HPLC. The thermogravimetric analysis (TGA) indicated that the sample underwent fast weight loss from 241 °C, and the fastest decomposition happens at around 292 °C (Figure S5).

As shown in Figure 3A−C and Table S1, AuNPs, ALDB, and ALDB-AA displayed similar hydrodynamic sizes and morphology. Specifically, the hydrodynamic sizes of AuNPs, ALDB, and ALDB-AA were 14.0 ± 0.1, 14.0 ± 0.4, and 18.2 ± 0.1 nm, respectively. In terms of zeta potentials, the readings for these three nanoparticles were −2.49 ± 0.26, 22.32 ± 0.76, and −1.36 ± 0.37 mV, respectively. The negative zeta potential of AuNPs can be attributed to the citrate capping on the nanoparticle surfaces, while the positive zeta potential of ALDB arises from the positively charged quaternary ammonium salt in the LDB ligand. Although quaternary ammonium salt also exists in ALDB-AA, the almost fully ionized AA moiety neutralizes its positive charge because the dissociation constant ($pK_a$) of AA is 4.1, while phenylboronic acid is not ionized under a physiological environment because

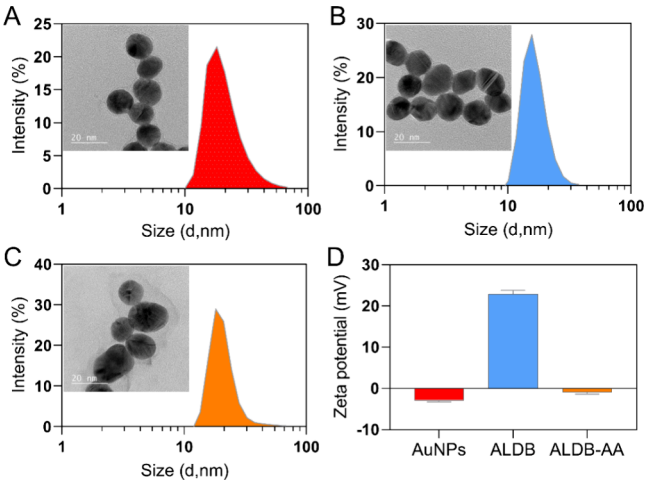


**Figure 3.** Size distribution and TEM image of (A) AuNPs, (B) ALDB, and (C) ALDB-AA. Scale bars = 20 nm. (D) Zeta potential of AuNPs, ALDB, and ALDB-AA.

its $pK_a$ is 8.8. As a result, the slightly negative zeta potential of ALDB-AA nanoparticles underscores the successful conjugation of AA to ALDB. This slightly negative zeta potential would facilitate tumor accumulation through an enhanced permeability and retention (EPR) effect.

To validate the dual stimuli-responsive behavior of the nanoprecursor, we investigated the pH-responsive AA release and ROS-responsive QM generation of ALDB-AA using a dialysis method, where AA release was detected by UV−vis spectroscopy and QM generation was determined by HPLC (Figure 4). The release of AA was significantly accelerated at

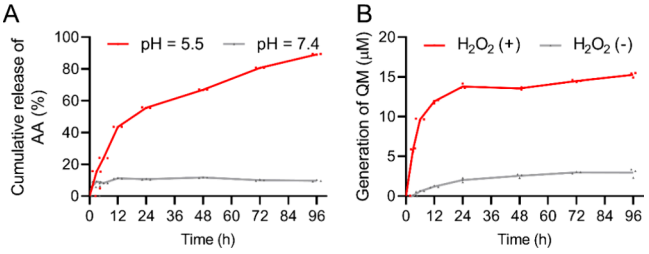


**Figure 4.** Dual stimuli-responsive behavior of the nanoprecursor. (A) Cumulative release of ascorbic acid from ALDB-AA at different pH values ($n$ = 3). (B) Generation of QM in the absence and presence of $H_2O_2$ ($n$ = 3).

pH = 5.5 compared with the physiological blood pH (7.4) (Figure 4A). Approximately 55% of AA was released within 24 h and over 90% by 96 h at pH 5.5. In contrast, less than 10% of loaded AA was released at pH = 7.4 after incubation for even 96 h. These results suggested that AA is predominantly released in more acidic microenvironments, which may selectively induce an excess amount of ROS generation under pathological conditions. The generation of QM in the presence of $H_2O_2$ almost finished within 24 h, whereas few QM was generated in the absence of $H_2O_2$, indicating that the generation of QM is highly dependent on the triggering of $H_2O_2$ (Figure 4B). These results validated the dual stimuli-responsive behavior of the nanoprecursor.

**Intracellular Oxidative Stress Induction by ALDB-AA.** To measure the intracellular ROS level induced by ALDB-AA, we qualitatively and quantitatively evaluated the total intra-


https://doi.org/10.1021/acsomega.4c04260
ACS Omega 2024, 9, 32124−32132

cellular ROS level in both HT29 and L929 cell lines using flow cytometry and confocal laser scanning microscopy (CLSM) (Figure 5).

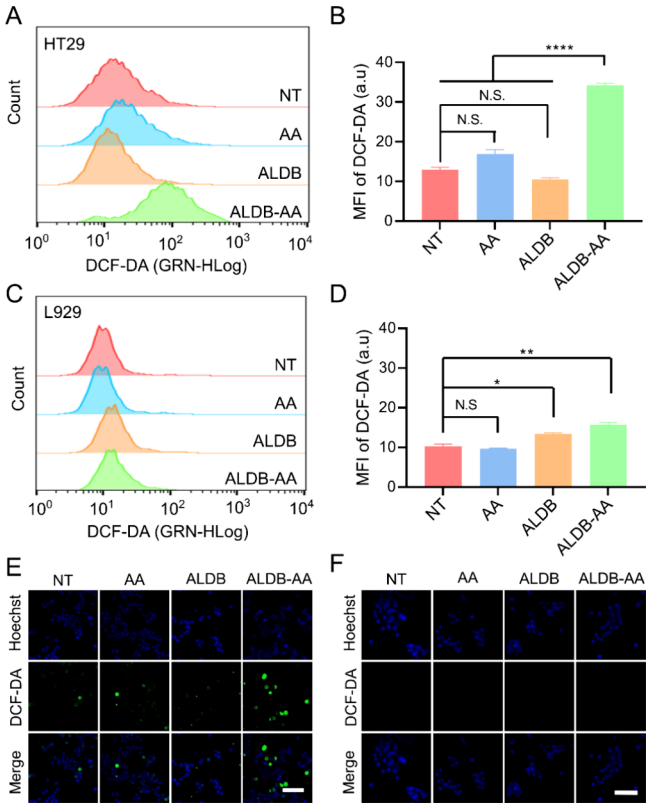


**Figure 5.** Intracellular oxidative stress by ALDB-AA. (A) Total intracellular ROS level in HT29 cells and (B) quantitative result of MFI ($n$ = 3) and L929 cells (C, D). Confocal fluorescence microscopy image of intracellular ROS in (E) HT29 cells and (F) L929 cells (scale bars: 30 $\mu$m).

With the increase in the particle size of AuNPs (20 nm), the cellular uptake was significantly enhanced in HT29 cells compared to L929 cells. Flow cytometry data (Figure 5A) revealed that free AA only marginally increased the ROS level in HT29 cells. This might indicate a very low intracellular AA concentration, likely resulting from the weak uptake of free AA. In contrast, cells treated with ALDB-AA showed a significantly higher ROS level. Quantitative analysis (Figure 5B) further confirmed that ALDB-AA amplified the total ROS level 3-fold. This significant increase in ROS with ALDB-AA can be attributed to the enhanced cellular uptake of AA, facilitated by the smaller size and pH-sensitive drug release of nanoparticles at tumor cell sites. No significant change in ROS levels was observed across all fibroblast cell groups, possibly due to the limited release of AA (Figure 5C,D). This observation is consistent with confocal laser scanning microscopy (Figure 5E,F), where ALDB-AA-treated HT29 cells displayed more intense fluorescence compared with normal cells. These findings signify that AA-conjugated nanoparticles could have enhanced selectivity toward tumor cells over normal cells.

**GSH Depletion by ALDB-AA.** To validate ALDB-AA, a tumor-specific GSH scavenger, we quantified the intracellular GSH content in cancer cells (HT29) and normal cells (L929) using flow cytometry. As shown in Figure 6A, both ALDB and ALDB-AA substantially reduce the intracellular GSH in HT29 cells. In contrast, cells treated with free AA exhibited GSH levels comparable to those of the control groups. Specifically, the ALDB-AA-treated group displayed a more significant GSH depletion than did the ALDB-treated groups, probably due to the enhanced ROS generation by AA, thereby boosting QM production at the cellular level. However, for normal cells, the GSH levels remained consistent across all groups and showed no significant deviation from the control groups (Figure 6B).

Overall, GSH depletion was predominantly observed in cancer cells, which inherently possess elevated ROS levels and a more acidic intracellular microenvironment. In the presence of high ROS levels, the phenylboronic group of ALDB readily reacts to generate QM molecules effectively. Therefore, the combined effects of ROS generation and QM production by AA and ALDB, respectively, selectively amplify oxidative stress, disrupting redox homeostasis in tumor cells.

***In Vitro* Cytotoxicity of ALDB-AA.** The above experimental results suggest that in response to intracellular pH and ROS, ALDB-AA undergoes degradation and amplifies oxidative stress in cancer cells. Moreover, ALDB generated a substantial number of QM molecules, leading to GSH depletion. The enhanced ROS level accompanied by the diminished antioxidant GSH level likely disrupted the redox homeostasis in cancer cells, resulting in cell death. To confirm the cytotoxic potential of ALDB-AA, its dose-dependent cytotoxicity in both tumor (HT29) and normal cells (L929) was further investigated (Figure 7). At concentrations higher than 25 $\mu$M in AA equiv, ALDB-AA starts to exhibit slight cytotoxicity toward cancer cells, and the viability of cancer cells is reduced to less than 30% when the concentration is higher than 200 $\mu$M in AA equiv. In comparison, no cytotoxicity was observed in normal cells even at concentrations of 1000 $\mu$M (AA equiv). Additionally, AA itself did not exhibit significant cytotoxicity even at 1000 $\mu$M, which agrees well with the previous reports that only when the concentrations of vitamin C are as high as 2−10 mM could selectively kill cancer cells.[30,31] This effect is caused by the synergistic effect of GSH depletion mediated by the generated QMs. This result can also be supported indirectly by the previous report from Chakraborty and Jana,[15] in which they used a similar formulation but 3-carboxy phenylboronic acid was used for AA conjugation. Their formulation induced cytotoxicity to cancer cells at 2−10 mM of AA because carboxy phenylboronic acid in the *meta*-position (3-position) was impossible to generate QMs by reacting with $H_2O_2$. Similarly, ALDB independently demonstrates minimal cytotoxicity at higher concentrations, indicating that the GSH depletion by QMs may affect cell viability. Particularly, ALDB-AA displayed enhanced cytotoxicity in HT29 cells compared to either free AA or ALDB. These results indicated the synergistic action of AA and ALDB in disrupting redox balance through augmented ROS production and GSH depletion. Conversely, normal cells (Figure 7B) maintained cell viability owing to lower ROS levels and a more neutral intracellular pH, which is less conducive to ROS and QM production.

We further validated the programmed cell death induced by redox imbalance in HT29 cells, caused by ALDB-AA, using flow cytometry with an annexin V/propidium iodide (PI) apoptosis detection kit (Figure 7C). While AA did not independently induce significant apoptosis, which is similar to the control group, ALDB prompted a moderate apoptotic response (28.0% early apoptosis and 5.53% late apoptosis), possibly due to GSH depletion by the generated QMs, as


https://doi.org/10.1021/acsomega.4c04260
ACS Omega 2024, 9, 32124−32132

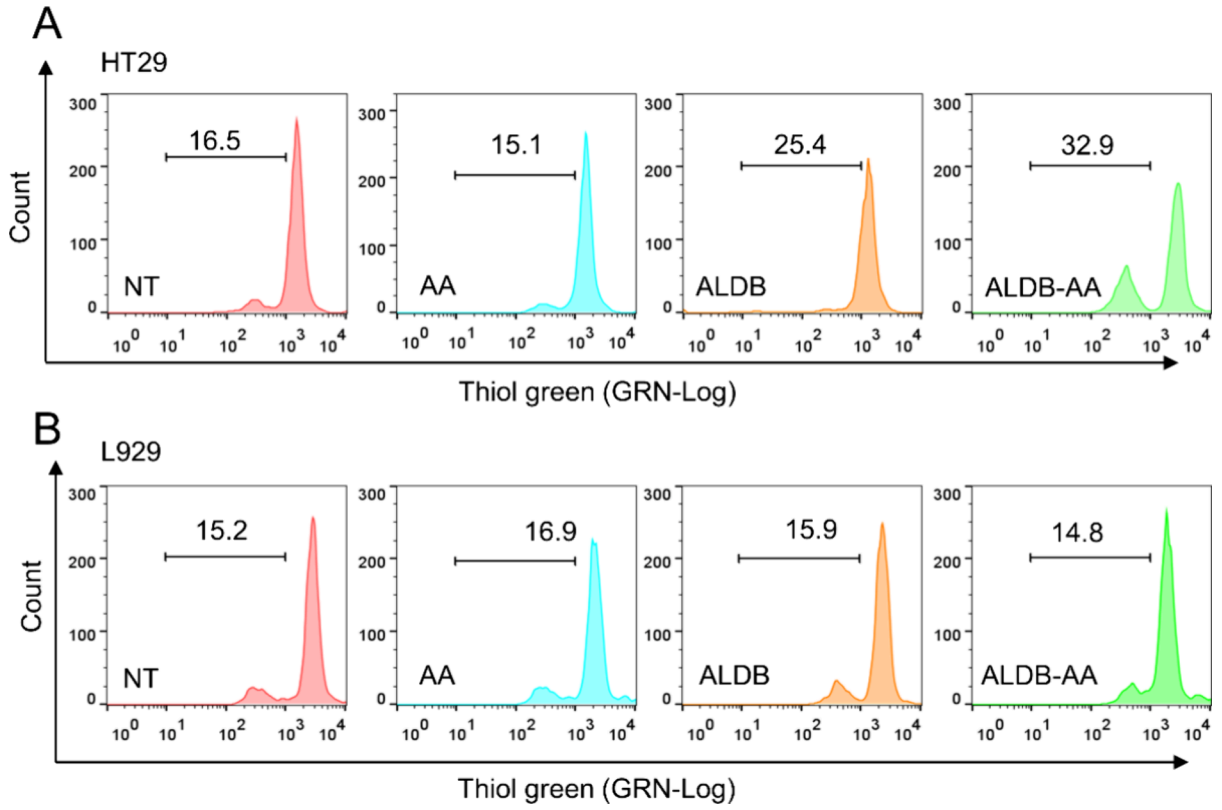


**Figure 6.** *In vitro* GSH depletion by ALDB-AA. Quantitative analysis of the intracellular GSH content using flow cytometry. (A) HT29 cells and (B) L929 cells. The experiment was performed using thiol green ($n$ = 3).

reported in previous studies.[26,32] Especially, ALDB-AA induced a higher apoptotic response (30.8% early apoptosis and 7.78% late apoptosis). This can be attributed to the synergistic effects of increased ROS production by AA and depletion of antioxidants (GSH) by QMs. These results emphasize that cells treated with ALDB-AA exhibit remarkably higher apoptosis rates compared with other groups.

To better understand the differences in the intracellular behaviors of nanoprecursors between cancer cells and normal cells, we investigated the intracellular concentration of nanoparticles by inductively coupled plasma mass spectrometry (ICP-MS) at different time points (Figure 8). The uptake efficiency in both cell lines increased similarly with time at 0−6 h. Interestingly, in contrast to the continuous accumulation of nanoparticles in cancer cells for 12 h of incubation, the concentration of nanoprecursors decreased in L929 cells at 12 h. It is unclear why this happened; a possible explanation might be that the nanoparticles underwent changes in the physicochemical property due to the removal of ascorbic acid and quinone methide moieties in cancer cells, which might hinder their efflux from the cells. This phenomenon will be further studied in future research.

## CONCLUSIONS

We successfully synthesized AA-conjugated Au nanoparticles, which are dual-responsive and release AA in response to acidic pH and produce QMs at elevated intracellular ROS levels selectively in cancer cells. These dual stimuli-responsive nanoparticles amplify ROS levels while simultaneously reducing intracellular GSH concentration. This synergistic effect of each component significantly accelerated oxidative stress and disrupted the redox homeostasis in cancer cells without affecting normal cells. The selective cytotoxicity to cancer cells could be achieved at a much lower concentration of AA compared to the existing reports. This advanced nanoparticle formulation heralds a promising avenue for antitumor therapy, leveraging the benefits of a minimal AA concentration and facilitating a new era of drug delivery and precise nanomedicine.

## EXPERIMENTAL PROCEDURE

**Materials.** DL-$\alpha$-Lipoic acid and triethylamine were obtained from Tokyo Chemical Industry Co. Ltd. (Tokyo, Japan). Gold(III) chloride trihydrate, methanesulfonyl chloride, 3-(dimethylamino)-1-propylamine, 4-(bromomethyl)-phenylboronic acid, trisodium citrate dihydrate, L-ascorbic acid, and 3-(4,5-dimethylthiazol-2-yl)-2,5-diphenyltetrazolium bromide (MTT) were from Sigma-Aldrich (St. Louis, MO, USA). Malignant (HT29) and fibroblast (L929) cell lines were purchased from the American Type Culture Collection (Manassas, VA, USA). RPMI 1640, Dulbecco's modified Eagle's medium (DMEM), and fetal bovine serum (FBS) were obtained from Capricorn Scientific (Ebsdorfergrund, Germany). Trypsin-EDTA, antibiotic-antimycotic solution, and phosphate-buffered saline (PBS) were acquired from Welgene (Daegu, Korea)

**Synthesis of 4-(Bromomethyl)phenylboronic Acid-Conjugated *N*-3-(Dimethylamino)-1-propyl Lipoamide (LDB).** LDB was synthesized through the routine shown in Figure S1. Lipoic acid (6.1 g, 0.03 mol) and $Et_3N$ (4.19 mL, 0.03 mol) were dissolved in $CH_2Cl_2$ (60 mL). The mixture was stirred in an ice bath under a nitrogen atmosphere for 30 min. Subsequently, methanesulfonyl chloride (2.32 mL, 0.03 mol) was added dropwise. The reaction mixture was gradually


https://doi.org/10.1021/acsomega.4c04260
ACS Omega 2024, 9, 32124−32132

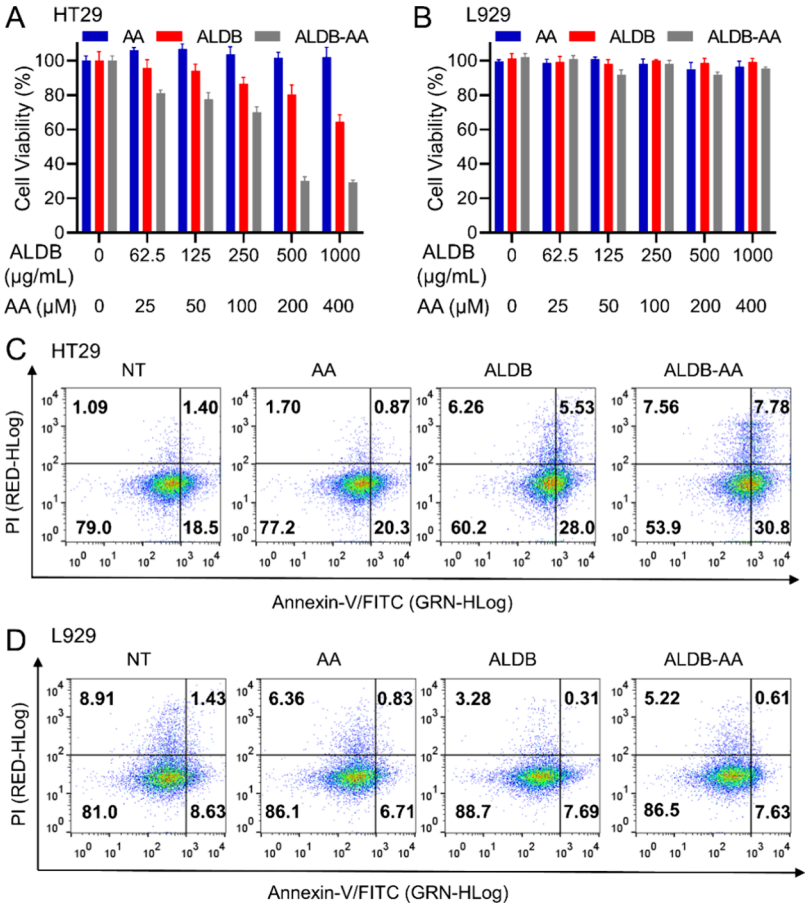


**Figure 7.** *In vitro* cytotoxicity of ALDB-AA. (A, B) Dose-dependent cell viability in (A) HT29 cells and (B) L929 cells measured by the MTT assay. Error bars represent the SD ($n$ = 5). (C, D) Typical scatter diagram of the annexin V/propidium iodide apoptosis assay generated from flow cytometry in HT29 cells (C) and L929 cells (D).

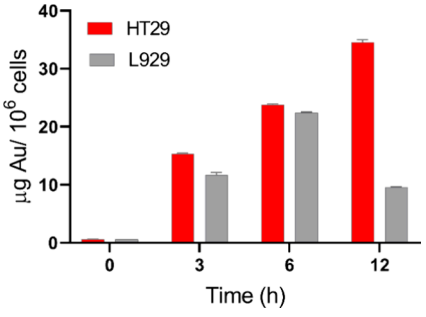


**Figure 8.** Intracellular level of ALDB-AA nanoprecursors in HT29 and L929 cells (presented by the mass of Au per $10^6$ cells). All data were obtained after treatment with nanoparticles at different time intervals, and each value represents an average ± SEM of three independent experiments.

heated and stirred for 5 h. Next, a solution of 3-(dimethylamino)-1-propylamine (3.05 mL, 0.02 mol) and $Et_3N$ (1.67 mL, 0.01 mol) in 40 mL of $CH_2Cl_2$ was added into the solution dropwise (over 30 min) under a nitrogen atmosphere and the reaction mixture was stirred overnight. Thereafter, the reaction mixture was washed with water (60 mL, two times) and saturated $Na_2CO_3$ solution. The organic layer was dried using $MgSO_4$ and filtered, with the solvent removed using a rotary evaporator. *N*-3-(Dimethylamino)-1-propyl lipoamide (LD) was obtained as a white solid (yield 83.62%).

Then, 4-(bromomethyl)phenylboronic acid (234 mg, 1.1 mmol) was added to LD (160 mg, 0.55 mmol) in a DMF (6 mL) solution, and the mixture was stirred overnight at room temperature. The end product was obtained by precipitation in ether and dried in a vacuum oven (yield 89.07%).

The LDB and intermediate structure were confirmed by $^1H$ NMR (Figures S2 and S3). Each peak was assigned well, indicating the successful synthesis of the LDB. EDS mapping confirmed the existence of both Au and S elements.

**Formulation of Gold Nanoparticles (AuNPs).** Gold nanoparticles were synthesized by reducing $AuCl_3$ using citrate in boiling water. $AuCl_3$ (9.8 mg, 0.032 mmol) was dissolved in 100 mL of deionized water. At the boiling point, sodium citrate (34 mg, 0.12 mmol) was rapidly introduced into the solution, accompanied by vigorous stirring. The solution was continuously heated until its color changed to wine red. The nanoparticles were then dialyzed (MWCO = 12 kDa) against deionized water for 3 days by changing the water thrice daily.

**Preparation of LDB-Conjugated Gold Nanoparticles (ALDB).** LDB (5 mg) was mixed with AuNPs (5 mg) in 50 mg of deionized water at a pH of 8.0. The mixture was stirred overnight at room temperature under dark conditions. Thereafter, the nanoparticle was dialyzed (MWCO = 12 kDa) against deionized water for 3 days by changing the water thrice daily.

**Synthesis of AA-Conjugated ALDB Nanoparticles (ALDB-AA).** An aqueous solution of AA (9.50 mg, 0.054 mmol, 1 mL) was added dropwise to 10 mg of ALDB solution,


https://doi.org/10.1021/acsomega.4c04260
ACS Omega 2024, 9, 32124−32132

and the pH of the solution was maintained at 7.4. The mixture was stirred for 6 h and centrifuged at 12,000 rpm to collect the nanoparticles. They were washed with water three times and finally resuspended in distilled water to a concentration of 2 mg/mL. The amount of AA conjugated to the nanoparticles was determined using UV−vis spectroscopy.

**TGA Analysis.** Thermogravimetric analysis of ALDB-AA was conducted using a Seiko Exstar 6000 TG analyzer with a heating rate of 20 °C/min, spanning from 25 to 800 °C under a $N_2$ atmosphere. The TGA analysis revealed that ALDB-AA degrades in a multiple-step process. Initially, decomposition initiates within the temperature range of 86−149 °C. This initial weight loss is attributed to the presence of moisture in the samples, while degradation takes in the range of 241−800 °C approximately with a maximum decomposition temperature of around 292 °C.

***In Vitro* QM Generation.** The production of QM from ALDB was assessed by HPLC analysis. A solution of ALDB at a concentration of 1 mg/mL was enclosed in a dialysis tube with a molecular weight cutoff (MWCO) of 1 kDa and dialyzed against an aqueous solution with or without hydrogen peroxide ($H_2O_2$). Samples were collected at designated time intervals. Quantification of generated QM was achieved by measuring the derivative of 4-hydroxybenzyl alcohol using HPLC under the following conditions: C18 column dimensions of 4.6 × 150 mm with a particle size of 5 μm, mobile phase composed of methanol and water in a ratio of 9:1 (v/v), flow rate set at 1 mL/min, and detection wavelength set at 240 nm using UV−vis spectroscopy.

**pH-Dependent AA Release.** The dialysis method was used to study the *in vitro* AA release behavior. Briefly, ALDB-AA was placed in a dialysis membrane (MWCO = 1 kDa). The membrane was immersed in PBS at different pH levels (pH = 7.4 and 5.5). The samples were maintained at 37 °C and gently shaken at 100 rpm. Fresh media were replaced at specific time intervals, and the concentration of AA was determined using UV−vis spectroscopy to plot the release curve.

**Cellular Uptake Studies.** Cellular uptake of ALDB-AA was assessed through an ICP-MS analysis. HT29 and L929 cells ($1 \times 10^6$ cells) were seeded in six-well plates and incubated for 24 h. A solution containing ALDB-AA nanoparticles (20 mg/L Au) was then added to both cell types for 3, 6, and 12 h durations. Control samples without nanoparticles were also prepared. Following the respective incubation periods, cells were washed with 1 mL of PBS and detached using trypsin-EDTA solution. Cell pellets were obtained by centrifugation at 1500 rpm for 5 min. These pellets were then resuspended in 1 mL of a serum-free culture medium, and cell counts were determined by using trypan blue staining and counting slides to ensure equal cell concentrations in each well. Subsequently, 2 mL of the culture medium was added to each vial and the samples were frozen. All samples underwent digestion using aqua regia in a microwave for 30 min, gradually increasing the temperature from 50 to 190 °C. The gold (Au) concentration was measured by ICP-MS (Nexlon 2000, PerkinElmer, USA) after dilution with a rhodium internal standard.

**Measurement of Total ROS.** The HT29 and L929 cells ($4 \times 10^5$ cells) were cultured in a six-well culture plate for 24 h and treated with free AA, ALDB, or ALDB-AA for 6 h. The cells were washed with DPBS and incubated with 10 μM of DCFH-DA (Sigma-Aldrich, St Louis, MO) in the dark at 37 °C for 30 min. Following incubation, they were detached and collected using trypsin-EDTA. The stained cells were analyzed by flow cytometry (Guava Easycyte, Merck Millipore, Germany).

**Confocal Imaging.** The HT29 and L929 cells ($2 \times 10^5$ cells) were seeded in confocal dishes for 24 h and incubated with free AA, ALDB, or ALDB-AA for 6 h. Thereafter, they were washed with DPBS and incubated with DCFH-DA (10 μM) for 30 min. The cells were stained with Hoechst solution and imaged by confocal microscopy (TCS SP8 HyVolution, Leica Microsystems CMS GmbH, Germany).

**Measurement of the Intracellular GSH level.** The intracellular GSH level was determined by flow cytometry using an intracellular GSH assay kit (ab112132, Abcam, USA). The HT29 and L929 cells ($2 \times 10^5$ cells) were seeded in a six-well plate for 24 h and incubated with free AA, ALDB, or ALDB-AA for 6 h. The cells were collected with trypsin-EDTA and washed with serum-containing media prior to incubation with a Thiol Green Dye-loading solution for 30 min. Thereafter, the cells were centrifuged at 1000 rpm for 4 min and resuspended in 1 mL of assay buffer, and the fluorescence intensity was assessed through flow cytometry.

***In Vitro* Cytotoxicity.** The cytotoxicity of ALDB-AA was determined by the MTT assay. Briefly, the HT29 and L929 cells were seeded in 96-well plates at a density of $1 \times 10^4$ cells per well and incubated for 24 h. They were incubated with various concentrations of AA, ALDB, or ALDB-AA for 24 h. MTT solution (100 μL) was added to each well and was incubated for 4 h. Thereafter, 200 μL of DMSO was added to each well, and the absorbance at 570 nm was measured using a microplate reader. The cell viability was determined by comparing the absorbance of the sample-treated cells and control cells.

**Annexin V/propidium Iodide Apoptosis Assay.** Tumor cell apoptosis was evaluated using an annexin V-fluorescein isothiocyanate (FITC) apoptosis detection kit (Thermo Fisher Scientific, USA). The cells were seeded in a six-well plate ($4 \times 10^5$ cells per well) for 24 h and incubated with various concertations of AA, ALDB, or ALDB-AA for 24 h. The cells were then collected, washed with PBS, and resuspended in the binding buffer at a concentration $1\times 10^6$ cells/mL. Subsequently, apoptosis was determined by adding the apoptosis detection kit and following the instructions provided by the manufacturer.

**Statistical Analysis.** All the values were indicated as the mean ± standard deviation (SD). The statistical analysis among each group was calculated by one-way analysis of variance (ANOVA) for multiple group comparisons, and Student's *t*-tests were used for two-group comparisons. Differences with $p < 0.05$ were considered statistically significant. The statistical significance was determined as $^*p < 0.05$, $^{**}p < 0.01$, $^{***}p < 0.005$, and $^{****}p < 0.001$.

## ■ ASSOCIATED CONTENT

### Supporting Information

The Supporting Information is available free of charge at https://pubs.acs.org/doi/10.1021/acsomega.4c04260.

Synthesis route of LDB, $^1$H NMR spectra of LD and LDB, and characterization of nanoparticles (PDF)



https://doi.org/10.1021/acsomega.4c04260
ACS Omega 2024, 9, 32124−32132

## AUTHOR INFORMATION


### Corresponding Authors

**Yuce Li** − *School of Chemical Engineering, College of Engineering, Sungkyunkwan University (SKKU), Suwon 16419, Republic of Korea; College of Life Sciences and Health, Wuhan University of Science and Technology (WUST), Wuhan 430065, China;* orcid.org/0000-0003-0656-3149; Email: liyuce@wust.edu.cn

**Jae Hyung Park** − *School of Chemical Engineering, College of Engineering, Sungkyunkwan University (SKKU), Suwon 16419, Republic of Korea; Department of Health Sciences and Technology, Samsung Advanced Institute for Health Science & Technology (SAIHST), Sungkyunkwan University, Seoul 06355, Republic of Korea; Biomedical Institute for Convergence at SKKU (BICS), Sungkyunkwan University, Suwon 16419, Republic of Korea;* orcid.org/0000-0002-5043-9455; Email: jhpark1@skku.edu

### Authors

**Anup Dey** − *School of Chemical Engineering, College of Engineering, Sungkyunkwan University (SKKU), Suwon 16419, Republic of Korea*

**Pramod Kumar E. K.** − *School of Chemical Engineering, College of Engineering, Sungkyunkwan University (SKKU), Suwon 16419, Republic of Korea*

**Chan Ho Kim** − *School of Chemical Engineering, College of Engineering, Sungkyunkwan University (SKKU), Suwon 16419, Republic of Korea;* orcid.org/0000-0001-7811-2254

Complete contact information is available at: https://pubs.acs.org/10.1021/acsomega.4c04260


### Author Contributions

Y.L. and J.H.P. designed and supervised the study and revised the manuscript; A.D., Y.L., and C.H.K. performed the experiments; A.D., Y.L., and P.K.E.K. analyzed the experimental data.

### Notes

The authors declare no competing financial interest.

## ACKNOWLEDGMENTS

This research was supported by the Korea Drug Development Fund (no. HN22C0624000022) funded by the Ministry of Science and ICT, Ministry of Trade, Industry and Energy, and Ministry of Health and Welfare, Republic of Korea. This work was also funded by the National Research Foundation of Korea (NRF) grant funded by the Korean government (MSIT) (no. RS-2023-00256265). The authors also thank the support from the Wuhan Science and Technology Bureau, China (grant no. 2023020201020405).

## REFERENCES


(1) Perillo, B.; Di Donato, M.; Pezone, A.; Di Zazzo, E.; Giovannelli, P.; Galasso, G.; Castoria, G.; Migliaccio, A. ROS in cancer therapy: the bright side of the moon. *Exp. Mol. Med.* **2020**, *52* (2), 192−203.

(2) Le Gal, K.; Schmidt, E. E.; Sayin, V. I. *Cellular Redox Homeostasis. Antioxidants* **2021**, *10* (9), 1377.

(3) Trachootham, D.; Lu, W.; Ogasawara, M. A.; Valle, N. R.-D.; Huang, P. Redox regulation of cell survival. *Antioxid. Redox Signaling* **2008**, *10* (8), 1343−1374.

(4) Giannoni, E.; Buricchi, F.; Grimaldi, G.; Parri, M.; Cialdai, F.; Taddei, M. L.; Raugei, G.; Ramponi, G.; Chiarugi, P. Redox regulation of anoikis: reactive oxygen species as essential mediators of cell survival. *Cell Death Differ.* **2008**, *15* (5), 867−878.

(5) Bhattacharyya, A.; Chattopadhyay, R.; Mitra, S.; Crowe, S. E. Oxidative stress: an essential factor in the pathogenesis of gastrointestinal mucosal diseases. *Physiol. Rev.* **2014**, *94* (2), 329−354.

(6) Xing, F.; Hu, Q.; Qin, Y.; Xu, J.; Zhang, B.; Yu, X.; Wang, W. The Relationship of Redox With Hallmarks of Cancer: The Importance of Homeostasis and Context. *Front. Oncol.* **2022**, *12*, No. 862743.

(7) Saleh, E. A. M.; Al-dolaimy, F.; Qasim almajidi, Y.; Baymakov, S.; kader M, M. A.; Ullah, M. I.; Abbas, A. h. R.; Khlewee, I. H.; Bisht, Y. S.; Alsaalamy, A. H. Oxidative stress affects the beginning of the growth of cancer cells through a variety of routes. *Pathol., Res. Pract.* **2023**, *249*, No. 154664.

(8) Li, Y.; Zhang, X.; Wang, Z.; Li, B.; Zhu, H. Modulation of redox homeostasis: A strategy to overcome cancer drug resistance. *Front. Pharmacol.* **2023**, *14*, 1156538.

(9) El-Hawiet, A.; Elessawy, F. M.; El Demellawy, M.; El-Yazbi, A. F. Green fast and simple UPLC-ESI-MRM/MS method for determination of trace water-soluble vitamins in honey: Greenness assessment using GAPI and analytical eco-scale. *Microchemical Journal* **2022**, *181*, No. 107625.

(10) Chen, Q.; Espey, M. G.; Krishna, M. C.; Mitchell, J. B.; Corpe, C. P.; Buettner, G. R.; Shacter, E.; Levine, M. Pharmacologic ascorbic acid concentrations selectively kill cancer cells: action as a pro-drug to deliver hydrogen peroxide to tissues. *Proc. Natl. Acad. Sci. U. S. A.* **2005**, *102* (38), 13604−13609.

(11) Chen, Q.; Espey, M. G.; Sun, A. Y.; Pooput, C.; Kirk, K. L.; Krishna, M. C.; Khosh, D. B.; Drisko, J.; Levine, M. Pharmacologic doses of ascorbate act as a prooxidant and decrease growth of aggressive tumor xenografts in mice. *Proc. Natl. Acad. Sci. U. S. A.* **2008**, *105* (32), 11105−11109.

(12) Pawlowska, E.; Szczepanska, J.; Blasiak, J. Pro- and Antioxidant Effects of Vitamin C in Cancer in correspondence to Its Dietary and Pharmacological Concentrations. *Oxid. Med. Cell. Longevity* **2019**, *2019*, 7286737.

(13) Dashty, M.; Motazacker, M. M.; Levels, J.; Vries, M. d.; Mahmoudi, M.; Peppelenbosch, M. P.; Rezaee, F. Proteome of human plasma very low-density lipoprotein and low-density lipoprotein exhibits a link with coagulation and lipid metabolism. *Thromb. Haemostasis* **2014**, *111* (3), 518−530.

(14) Santos, K. L. B.; Bragança, V. A. N.; Pacheco, L. V.; Ota, S. S. B.; Aguiar, C. P. O.; Borges, R. S. Essential features for antioxidant capacity of ascorbic acid (vitamin C). *J. Mol. Model.* **2021**, *28* (1), 1.

(15) Chakraborty, A.; Jana, N. R. Vitamin C-Conjugated Nanoparticle Protects Cells from Oxidative Stress at Low Doses but Induces Oxidative Stress and Cell Death at High Doses. *ACS Appl. Mater. Interfaces* **2017**, *9* (48), 41807−41817.

(16) Nita, M.; Grzybowski, A. The Role of the Reactive Oxygen Species and Oxidative Stress in the Pathomechanism of the Age-Related Ocular Diseases and Other Pathologies of the Anterior and Posterior Eye Segments in Adults. *Oxid. Med. Cell. Longevity* **2016**, *2016*, 3164734.

(17) Villalpando-Rodriguez, G. E.; Gibson, S. B.; Tejero, J. Reactive Oxygen Species (ROS) Regulates Different Types of Cell Death by Acting as a Rheostat. *Oxid. Med. Cell. Longevity* **2021**, *2021*, 9912436.

(18) Jena, A. B.; Samal, R. R.; Bhol, N. K.; Duttaroy, A. K. Cellular Red-Ox system in health and disease: The latest update. *Biomed. Pharmacother.* **2023**, *162*, No. 114606.

(19) Hwang, C.; Sinskey, A. J.; Lodish, H. F. Oxidized redox state of glutathione in the endoplasmic reticulum. *Science* **1992**, *257* (5076), 1496−1502.

(20) Espinosa-Diez, C.; Miguel, V.; Mennerich, D.; Kietzmann, T.; Sanchez-Perez, P.; Cadenas, S.; Lamas, S. Antioxidant responses and cellular adjustments to oxidative stress. *Redox Biol.* **2015**, *6*, 183−197.

(21) Ghanbari Movahed, Z.; Rastegari-Pouyani, M.; Mohammadi, M. H.; Mansouri, K. Cancer cells change their glucose metabolism to overcome increased ROS: One step from cancer cell to cancer stem cell? *Biomed. Pharmacother.* **2019**, *112*, No. 108690.

(22) Schieber, M.; Chandel, N. S. ROS function in redox signaling and oxidative stress. *Curr. Biol.* **2014**, *24* (10), R453−462.
(23) Cockfield, J. A.; Schafer, Z. T. Antioxidant Defenses: A Context-Specific Vulnerability of Cancer Cells. *Cancers* **2019**, *11* (8), 1208.
(24) Tan, S.; Sagara, Y.; Liu, Y.; Maher, P.; Schubert, D. The regulation of reactive oxygen species production during programmed cell death. *J. Cell Biol.* **1998**, *141* (6), 1423−1432.
(25) Dey, A.; Jeon, J.; Yoon, B.; Li, Y.; Park, J. H. Cascade-amplified self-immolative polymeric prodrug for cancer therapy by disrupting redox homeostasis. *J. Controlled Release* **2023**, *358*, 555−565.
(26) Jeon, J.; Yoon, B.; Dey, A.; Song, S. H.; Li, Y.; Joo, H.; Park, J. H. Self-immolative polymer-based immunogenic cell death inducer for regulation of redox homeostasis. *Biomaterials* **2023**, *295*, No. 122064.
(27) Pan, Q.; Zhang, B.; Peng, X.; Wan, S.; Luo, K.; Gao, W.; Pu, Y.; He, B. A dithiocarbamate-based H2O2-responsive prodrug for combinational chemotherapy and oxidative stress amplification therapy. *Chem. Commun.* **2019**, *55* (92), 13896−13899.
(28) Noh, J.; Kwon, B.; Han, E.; Park, M.; Yang, W.; Cho, W.; Yoo, W.; Khang, G.; Lee, D. Amplification of oxidative stress by a dual stimuli-responsive hybrid drug enhances cancer cell death. *Nat. Commun.* **2015**, *6* (1), 6907.
(29) Köse, D. A.; Zümreoglu-Karan, B. Complexation of boric acid with vitamin C. *New J. Chem.* **2009**, *33* (9), 1874−1881.
(30) Uetaki, M.; Tabata, S.; Nakasuka, F.; Soga, T.; Tomita, M. Metabolomic alterations in human cancer cells by vitamin C-induced oxidative stress. *Sci. Rep.* **2015**, *5*, 13896.
(31) Böttger, F.; Vallés-Martí, A.; Cahn, L.; Jimenez, C. R. High-dose intravenous vitamin C, a promising multi-targeting agent in the treatment of cancer. *J. Exp. Clin. Cancer Res.* **2021**, *40* (1), 343.
(32) Sun, Y.; Zheng, Y.; Wang, C.; Liu, Y. Glutathione depletion induces ferroptosis, autophagy, and premature cell senescence in retinal pigment epithelial cells. *Cell Death Dis.* **2018**, *9* (7), 753.


https://doi.org/10.1021/acsomega.4c04260
*ACS Omega* 2024, 9, 32124−32132